Journal of Materials Chemistry A

ROYAL SOCIETY OF CHEMISTRY

COMMUNICATION

View Article Online
View Journal | View Issue

Cite this: J. Mater. Chem. A, 2024, 12, 23406

Received 20th June 2024
Accepted 31st July 2024

DOI: 10.1039/d4ta04268a

rsc.li/materials-a

Facets in metal halide perovskite nanocrystals for the photoinduced electron transfer annulation reaction†

Qing Guo, ‡*[a] Jun-Lin Lu,‡[a] Bin Qin,[b] Qi-Chao Shan,[a] Le Liu, [a] Jin-Dan Zhang,[a] Xi Liu,*[c] Xin-Hua Duan [a] and Li-Na Guo*[a]

Facet engineering has been confirmed as a feasible method to regulate the performance of photocatalysts. Here we take photoinduced decarboxylative cyclization of *N*-aryl glycine and *N*-aryl maleimide as a model reaction to explore the influence of metal halide perovskite nanocrystal facets on the photocatalytic performance of organic synthesis. In terms of promoted charge-carrier dynamics and the suitable adsorption potentials for the substrate and intermediate, cubes with four (110) and two (002) facets exhibited higher activity for photocatalytic cascade cyclization than polyhedra.

Owing to their unique and excellent optoelectronic properties,[1] metal halide perovskite (MHP) nanocrystals (NCs) have sparked great interest and become one of the most promising candidates for optoelectronic applications, including light-emitting diodes,[2,3] photodetectors,[4,5] lasers[6] and solar cells.[7–10] In addition, due to their processability, intriguing photophysical and transport properties (*i.e.*, high molar extinction coefficients and adjustable bandgap), long charge-carrier lifetime, long carrier diffusion lengths, and unique tolerance to defects,[11–13] MHP materials have gained prominence in the field of photochemical applications, such as hydrogen generation,[14] CO_2 reduction,[15] and organic synthesis[16–18] in recent years, since the first report of halide perovskites for photocatalysis in 2016.[19] Unfortunately, the efficiency associated with these photocatalytic systems is unsatisfactory, mainly because of poor photogenerated carrier separation efficiency and limited reactive sites.

Facet engineering holds great potential in the modulation of photocatalytic performance of photocatalysts by exposing different active sites on their surface,[20] which has been proved for TiO_2,[21,22] Cu_2O, metal–organic frameworks[23] and so on. For example, Rajh *et al.* reported that the (110) facet of a single Cu_2O photocatalyst particle could reduce CO_2 to methanol while the (100) facet was inert under illumination.[24] In addition, Sun *et al.* found that the relative ratio of (111) and (101) facets exposed on Fe-soc-MOFs has an influence on the activity and selectivity of photoreduction CO_2 to CO.[23] Moreover, Wang *et al.* successfully controlled the selectivity in photocatalytic oxidation of biopolyols to formic acid or CO through selective exposing the (001)/(101) facet of TiO_2.[25] Due to the different atomic arrangement and electronic structures, different crystal facets of photocatalysts exhibit different reactivity and surface physical/chemical properties.[26] Therefore, facet engineering could realize the distribution of reactive sites and transport of the surface charge, leading to the regulation of photocatalytic performance. Although great efforts have been devoted to the modulation of photocatalytic performance, to the best of our knowledge, the strategy of facet engineering is just being adopted in the fields of CO_2 reduction, H_2 evolution and dye degradation,[27] while it has rarely been studied in organic synthesis.

Aza-heterocycles are a class of important units, which widely exist in various natural products, agrochemicals, pharmaceuticals, and organic functional materials. According to reports, 59% of US FDA-approved medicines are composed of nitrogen heterocycles.[28,29] Due to their importance, the construction of nitrogen-containing heterocycles has received extensive attention in recent years. Among various strategies, the cascade cyclization reaction has become a valuable approach, which has shown step-economy and operational simplicity.[30,31] Thus, we chose the photoinduced decarboxylative cyclization of *N*-aryl glycines and *N*-aryl maleimides as a model reaction to

[a]*Xi'an Key Laboratory of Sustainable Energy Material Chemistry, Engineering Research Center of Energy Storage Materials and Devices, School of Chemistry, Xi'an Jiaotong University, Xi'an, 710049, P. R. China. E-mail: guoqing92@xjtu.edu.cn; guoln81@xjtu.edu.cn*

[b]*Department of Chemistry, The University of Hong Kong, Hong Kong 999077, P. R. China*

[c]*Research Center for Tissue Repair and Regeneration Affiliated to the Medical Innovation Research Department, PLA General Hospital and PLA Medical College, Beijing, 100048, P. R. China. E-mail: liuxipla@163.com*

† Electronic supplementary information (ESI) available. See DOI: https://doi.org/10.1039/d4ta04268a

‡ These authors contributed equally to this work.

investigate the influence of MHP NC facets on the photocatalytic performance of organic synthesis.

Herein, two different morphologies of $CsPbBr_3$ NCs with different exposed crystal facets were prepared, namely, cube, and polyhedron, which are referred to as Cube, and Poly, respectively. The results of photocatalytic cyclization of *N*-phenyl glycine **1a** and *N*-phenyl maleimide **2a** shown that Cube with exposed four (110) and two (002) facets gave a higher yield (75%) of the aza-heterocycle product than Poly (33%) with exposed four (110), two (002), eight (112), eight (012), and four (100) facets. This indicated that facet-engineering of MHP NCs is feasible to modulate the photocatalytic performance of organic synthesis. Mechanistic insights indicated that the higher photocatalytic activity benefits from the facile photoinduced interfacial electron transfer from Cube to the substrate, as well as more favorable adsorption of *N*-aryl glycine and easier desorption of intermediates on (110) and (002) facets of Cube.

The preparation of $CsPbBr_3$ NCs with different crystal facets was achieved according to previous reports,[32,33] and the shape was regulated *via* controlling the temperature of seed cluster injection and the reaction time (see details in the ESI†). As shown in Fig. 1b, $CsPbBr_3$ NCs obtained at low injection temperature with shorter reaction time had the shape of a cube (denoted as Cube) with an average size of ~20 nm. The lattice spacings of 5.89 and 5.57 Å (Fig. 1c) were ascribed to the (001) and (110) planes of monoclinic $CsPbBr_3$, respectively. The selected area fast Fourier transform (FFT) pattern from the HRTEM image in Fig. 1c suggested the shape of the Cube was four planes of (110) and two (002) with zone axis [110] (Fig. S1, ESI†). However, $CsPbBr_3$ nanocubes turned to polyhedron-shaped NCs (denoted as Poly), which had the shape of corner-truncated cube with a size of ~25 nm with injection at higher temperature and prolonged reaction time (Fig. 1e). The redshifts of the first absorption peak in UV-vis absorption spectra (Fig. S2, ESI†) and the photoluminescence (PL) peak in PL spectroscopy (Fig. S3, ESI†) verified the larger size of Poly, because of the quantum confinement effect. Fig. 1f shows *d*-spacings of the perpendicular planes to be ~5.81 and ~5.95 Å, confirming that these were (110) and (002) planes. Planes with 45° were (112) planes with ~4.2 Å with the [110] zone axis. The corresponding FFT pattern is displayed in Fig. S4.† The geometric models were drawn according to previous reports[33] and shown in Fig. 1a and d. Moreover, the full X-ray photoelectron spectroscopy (XPS) spectrum implied the coexistence of Cs, Pb and Br elements (Fig. S5, ESI†), and high-resolution XPS spectra of Cs 3d, Pb 4f and Br 3d showed no obvious changes (Fig. S6, ESI†). In addition, the X-ray diffraction (XRD) pattern also confirmed the successful preparation of $CsPbBr_3$ NCs (Fig. S7, ESI†), in which the narrow peaks matched well with the standard pattern of monoclinic $CsPbBr_3$ (JCPDS No. 18-0364). The diffraction peaks almost remained unchanged after morphology regulation, suggesting that the crystal structure of NCs was retained. These results implied that two types of $CsPbBr_3$ NCs with exposed different facets were successfully synthesized. Subsequently, a ligand exchange was involved to replace the long-chain organic ligands on $CsPbBr_3$ NCs, because of their poor electrical conductivity, with tetrafluoroborate salt (NH_4BF_4).[34,35] The Fourier transform-infrared (FT-IR) spectra (Fig. S8, ESI†) shows the reduced density of organic ligands after ligand exchange, indicating the effective removal of organic ligands from the surface of NCs.

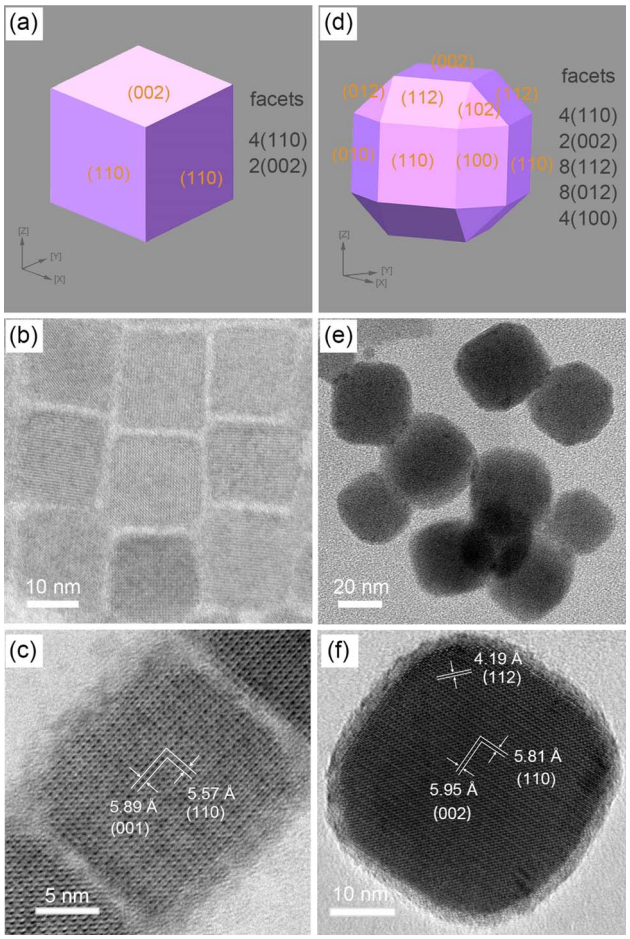

Fig. 1 (a) Geometric model, (b) transmission electron microscopy (TEM) image and (c) corresponding high-resolution TEM image of Cube. (d) Geometric model, (e) TEM image and (f) corresponding high-resolution TEM image of Poly.

Our initial attempt was to choose *N*-phenyl glycine **1a** and *N*-phenyl maleimide **2a** as model substrates in the presence of Cube in ethyl acetate (EA) at room temperature (Table 1). Upon irradiation of the reaction mixture with 10 W blue LEDs ($\lambda = 450$ nm) in air for 1 h, the desired heterocyclic product **3a** was obtained with 78% yield (Table 1, entry 1). Screening of solvents, including 1,4-dioxane, MTBE, THF, DCM, DCE and CH_3CN showed that EA was the best one (Table 1, entries 1–7). Control experiments showed that NCs, visible light, and the air atmosphere were all essential for this transformation (Table 1, entries 8–10). Satisfactorily, reducing the amount of **1a** to 2.0 equiv. (Table S1, ESI†) and the amount of Cube to 3 mg (Table S2, ESI†) still gave a comparable yield (75%) of **3a** (entry 11) because of scattering of light by much heterogeneous photocatalysts. In contrast, Poly showed a relatively lower catalytic reactivity for the formation of **3a**, giving only a yield of 33% (entry 12). The results indicated that $CsPbBr_3$ NCs with different

Table 1 Optimization of photocatalytic cascade cyclization

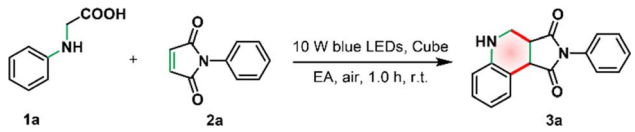

Entry	Variation from standard conditions[a]	Yields[b] (%)
1	None	78
2	1,4-Dioxane instead of EA	72
3	MTBE instead of EA	75
4	THF instead of EA	57
5	DCM instead of EA	45
6	DCE instead of EA	72
7	CH_3CN instead of EA	Trace
8	Without Cube	n.d.
9	Without light	n.d.
10	N_2 instead of air	n.d.
11[c]	2.0 equiv. of **1a**, and 3 mg Cube	75
12[c]	Poly instead of Cube	33
13[d]	Cube with organic ligands	30
14	BHT (2.0 equiv.)	60

[a] Reaction conditions: **1a** (0.6 mmol, 3.0 equiv.), **2a** (0.2 mmol, 1.0 equiv.), and Cube (6 mg) in EA (3.0 mL), with 10 W blue LED ($\lambda = 450$ nm) irradiation, at room temperature, under air for 1.0 h. [b] Yields were determined by ^{1}H NMR using 1,3,5-trimethoxybenzene as an internal standard. [c] **1a** (0.4 mmol, 2.0 equiv.), **2a** (0.2 mmol, 1.0 equiv.), and $CsPbBr_3$ (3 mg). [d] Cube with original ligands (3 mg).

exposed facets have a significant influence on the photocatalytic performance in organic synthesis. Moreover, the much lower yield of 30% for NCs with original ligands indicated the necessity of ligand exchange (entry 13).

To further demonstrate the generality of the facet-engineering strategy for this cyclization reaction, a series of *N*-aryl glycines and *N*-aryl maleimides were investigated under the optimal conditions. As shown in Fig. 2a, when Cube was used as the photocatalyst, a wide range of *N*-aryl amino acids **1a–1h** reacted with *N*-phenyl maleimide **2a** to give the desired products with much higher yields than that of using Poly as the photocatalyst. *N*-aryl amino acids bearing alkyl and alkoxy groups at the *p*-position of the aromatic ring afforded the corresponding products in very different yields ($yield_{Cube}/yield_{Poly}$) with Cube and Poly, respectively (**1a**, 75%/33%; **1b**, 96%/55%; **1c**, 81%/60%; **1d**, 66%/33%). A strong electron-withdrawing group, namely trifluoromethoxy, was also tolerated (**1e**, 90%/60%). Notably, substrates with halogen (F, Cl and Br) substituents showed a similar trend of influence for Cube and Poly photocatalysis (**1f**, 69%/48%; **1g**, 81%/69%; **1h**, 75%/54%). Next, a variety of maleimides **2** bearing aryl or benzyl groups on the nitrogen atom were examined (Fig. 2b). As shown in Fig. 2b, Cube exhibited higher photocatalytic activity for phenyl-substituted maleimide (**2a**) compared to Poly, and 75% and 33% yields were obtained, respectively. As expected, for the *p*-alkyl, and *p*-alkoxy substituted substrates, Cube also afforded the corresponding products **3** in higher yields, 90% (**2b**), 87% (**2c**), and 87% (**2d**). In contrast, when Poly was used as the photocatalyst, the yields were much lower (**2b**, 60%; **2c**, 57%; **2d**,

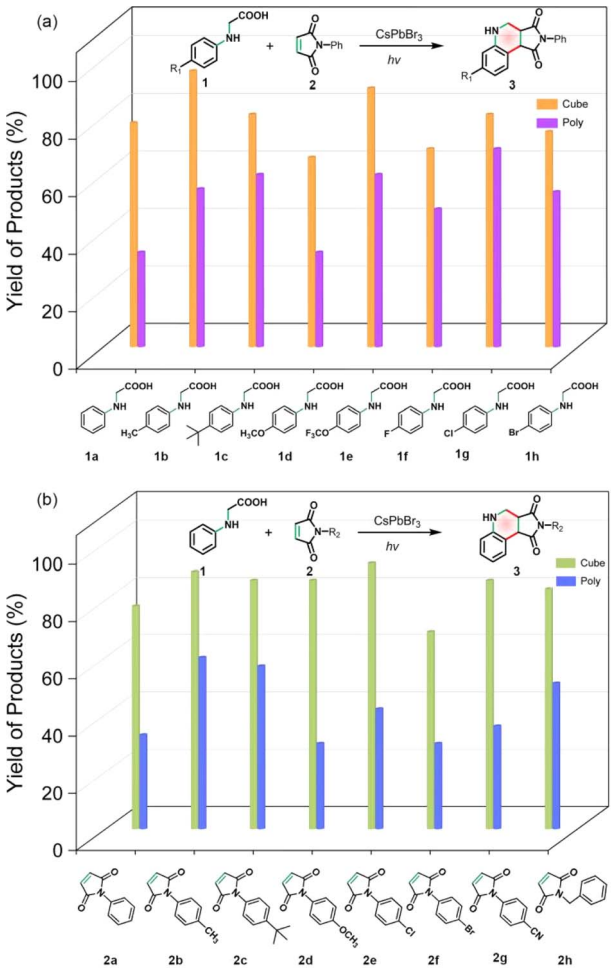

Fig. 2 Substrate scope for (a) **1** and (b) **2** with Cube and Poly as photocatalysts, respectively. Reaction conditions: **1** (0.4 mmol, 2.0 equiv.), **2** (0.2 mmol, 1.0 equiv.), $CsPbBr_3$ photocatalyst (3.0 mg), in EA (3 mL) at room temperature with 10 W blue LEDs ($\lambda = 450$ nm) for 1.0 h under air. Yields of products were determined by ^{1}H NMR analysis with 1,3,5-trimethoxybenzene as an internal standard.

30%). In addition, substrates with electron-withdrawing groups such as halogens (Cl and Br) and the cyano group on the aromatic ring also gave the desired products in different yields when Cube and Poly were used separately as photocatalysts (**2e**, 93%/42%; **2f**, 69%/30%; **2g**, 87%/36%). Notably, for *N*-benzyl maleimide (**2h**), Cube gave the product in 84% yield, while Poly led to the product in 51% yield. All the above results implied that Cube exhibited better photocatalytic performance than Poly, showing the great potential of facet-engineering in regulating this cyclization reaction.

Encouraged by the above results, we attempted to explore the mechanism of boosted photocatalytic performance of Cube. First, we calculated the band gaps of Cube and Poly through *Tauc* plots (Fig. S9, ESI†) to be ~2.42 and ~2.35 eV, respectively. And valence-band (VB) XPS analysis (Fig. S10, ESI†) was utilized to reveal the VB potentials of NCs, in which they were determined to be ~1.76 and ~1.75 V *vs.* NHE (normal hydrogen electrode), respectively. Thus, conduction bands (CB) were

calculated to be −0.66 and −0.60 V *vs.* NHE for Cube and Poly. The corresponding band structure is displayed (Fig. S11, ESI†). Accordingly, the driving forces of reduction and oxidation reaction were enough for both Cube and Poly. To further investigate the charge separation behaviors, spectroscopy measurements were conducted. It was found that the PL intensity of Cube was much higher (Fig. 3a), indicating the efficiently inhibited recombination of photogenerated electron–hole pairs through non-radiative pathways. In addition, the prolonged PL lifetime of charge carriers (60.7 ns) fitted with three exponential components τ_1 (trap-assisted exciton recombination), τ_2 (exciton recombination) and τ_3 (free-carrier recombination),[36] would be consequently favorable to transfer to participate in subsequent surface reactions (Fig. 3b and Table S3, ESI†). In addition, the photocurrent response and electrochemical impedance spectra (EIS) were measured in $TBAPF_6$ acetonitrile solution to unveil the promoted charge dynamics (see details in the ESI†). As displayed in Fig. 3c, Cube showed a much higher transient current density than Poly under light irradiation, implying the enhanced charge separation over Cube. Furthermore, a smaller arc radius with a lower charge transfer resistance (R_{ct}) of 2319 Ω was observed for Cube in EIS Nyquist plots (Fig. 3d and Table S4, ESI†), suggesting the accelerated interfacial charge transfer over Cube. Furthermore, the promoted charge carrier dynamics of Cube with organic long-chain ligands than that of Poly exclude the influence of ligand exchange, indicating the origin of their structures (Fig. S12, S13, Tables S5 and S6, ESI†). These results manifested that Cube with a suitable band structure for accelerated electron–hole separation and charge transfer was one of the reasons for superior heterocyclic compound production.

Subsequently, to reveal the facet-dependent catalytic behavior of photocatalysts by DFT calculations, the reaction mechanism was identified. The addition of butylated hydroxytoluene (BHT), radical scavenger into the system could effectively inhibit heterocyclic compound production (Table 1, entry 14). And the adduct of BHT and the phenylaminomethyl radical was detected by HRMS (Fig. S14, ESI†). The results suggested that the reaction proceeded *via* radical intermediates. Thus, the elementary steps for the reaction of **1a** and **2a** on the surface of NCs were proposed. As shown in Fig. S15,† it involved following steps: (1) first, **1a** was activated and adsorbed on the surface of NCs to generate **1a***; (2) the adsorbed **1a*** generated phenylaminomethyl radical intermediate **I** through a single-electron transfer (SET) process with the release of CO_2 and a proton; (3) radical **I** added to **2a**, generating radical **II**; (4) radical **II** quickly coupled with another radical **I** to generate intermediate **III**, which was then oxidized to give the product **3a**. During this process, the adsorption behaviors of **1a** on (110), (002), (112), (012), and (100) facets were explored (Fig. S16a–e, see details in the ESI†). The corresponding adsorption energies were calculated to be −0.26, −0.38, 0.07, −0.03 and −0.38 eV, respectively (Table S7, ESI†), indicating that **1a** could adsorb on all facets of Cube, while it can only adsorb on less than 40% surfaces for Poly. In addition, with the smaller BET surface area (Table S8, ESI†), we could conclude that **1a** was more favorable to adsorb on Cube than Poly. Furthermore, the adsorption behavior of phenylaminomethyl radical intermediate **I** was also revealed (Fig. S16f–j and Table S9, ESI†), which was important for the desired product. The much lower adsorption energies on (110) and (002) facets indicated the less favorable adsorption of intermediate **I** onto the NC surface, thus making it easy to react with free **2a** in solution to generate **II** and avoid the further oxidation on the surface. These results support that Cube with four (110) and two (002) facets has a higher yield of the heterocyclic compound.

In summary, we have systematically demonstrated that facet engineering is a feasible method to regulate the active sites exposed on MHP NCs and adjust the photocatalytic performance of organic synthesis with superior activity. The results showed that Cube exhibited a higher catalytic activity for the photoinduced decarboxylative cyclization of the *N*-aryl glycine and the *N*-aryl maleimide cascade. Mechanistic insights revealed that the higher photocatalytic activity is attributed to the promoted photogenerated electron–hole separation and charge transfer induced by difference in facet exposure. DFT calculations further revealed different reaction yields derived from the different adsorption potentials of NC for *N*-phenyl glycine **1a** and intermediate **I**. Understanding the influence of MHP NC facets on photocatalytic cascade cyclization activity would provide new insights for tuning the photocatalytic performance of organic synthesis under mild conditions.

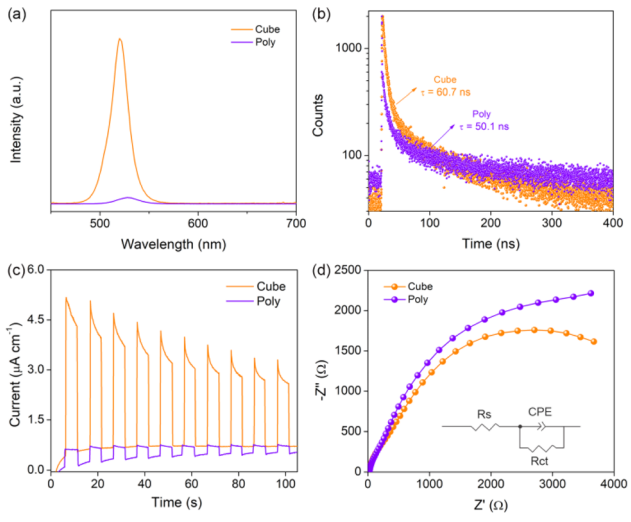

Fig. 3 (a) Steady-state PL spectra (excitation laser: 405 nm) and (b) time-resolved PL spectra of Cube and Poly. (c) Photocurrent responses and (d) EIS Nyquist plots of Cube and Poly electrodes (inset is the equivalent curve), respectively.

Data availability

The data that support the findings of this study are available from the corresponding authors upon reasonable request.

Conflicts of interest

There are no conflicts to declare.

Acknowledgements

We are grateful for financial support from the National Natural Science Foundation of China (No. 22302155), and the Fundamental Research Funds of the Center Universities (No. xzy01202202 and xtr072022003).

References

1 Y. Liu, S. Yuan, H. Zheng, M. Wu, S. Zhang, J. Lan, W. Li and J. Fan, *Adv. Energy Mater.*, 2023, **13**, 2300188.
2 A. Fakharuddin, M. K. Gangishetty, M. Abdi-Jalebi, S.-H. Chin, A. R. bin Mohd Yusoff, D. N. Congreve, W. Tress, F. Deschler, M. Vasilopoulou and H. J. Bolink, *Nat. Electron.*, 2022, **5**, 203–216.
3 B. Guo, R. Lai, S. Jiang, L. Zhou, Z. Ren, Y. Lian, P. Li, X. Cao, S. Xing, Y. Wang, W. Li, C. Zou, M. Chen, Z. Hong, C. Li, B. Zhao and D. Di, *Nat. Photonics*, 2022, **16**, 637–643.
4 Y. Zhang, Y. Ma, Y. Wang, X. Zhang, C. Zuo, L. Shen and L. Ding, *Adv. Mater.*, 2021, **33**, 2006691.
5 F. Wang, X. Zou, M. Xu, H. Wang, H. Wang, H. Guo, J. Guo, P. Wang, M. Peng, Z. Wang, Y. Wang, J. Miao, F. Chen, J. Wang, X. Chen, A. Pan, C. Shan, L. Liao and W. Hu, *Adv. Sci.*, 2021, **8**, 2100569.
6 H. Dong, C. Zhang, X. Liu, J. Yao and Y. S. Zhao, *Chem. Soc. Rev.*, 2020, **49**, 951–982.
7 X. Feng, Q. Guo, J. Xiu, Z. Ying, K. W. Ng, L. Huang, S. Wang, H. Pan, Z. Tang and Z. He, *Cell Rep. Phys. Sci.*, 2021, **2**, 100341.
8 N. K. Tailor, M. Abdi-Jalebi, V. Gupta, H. Hu, M. I. Dar, G. Li and S. Satapathi, *J. Mater. Chem. A*, 2020, **8**, 21356–21386.
9 T. Wu, X. Liu, X. Luo, X. Lin, D. Cui, Y. Wang, H. Segawa, Y. Zhang and L. Han, *Joule*, 2021, **5**, 863–886.
10 J. Y. Kim, J.-W. Lee, H. S. Jung, H. Shin and N.-G. Park, *Chem. Rev.*, 2020, **120**, 7867–7918.
11 J. Wang, Y. Shi, Y. Wang and Z. Li, *ACS Energy Lett.*, 2022, **7**, 2043–2059.
12 W. Song, G. Qi and B. Liu, *J. Mater. Chem. A*, 2023, **11**, 12482–12498.
13 K. Ren, S. Yue, C. Li, Z. Fang, K. A. M. Gasem, J. Leszczynski, S. Qu, Z. Wang and M. Fan, *J. Mater. Chem. A*, 2022, **10**, 407–429.
14 P. Zhou, H. Chen, Y. Chao, Q. Zhang, W. Zhang, F. Lv, L. Gu, Q. Zhao, N. Wang, J. Wang and S. Guo, *Nat. Commun.*, 2021, **12**, 4412.
15 Z. Liu, H. Yang, J. Wang, Y. Yuan, K. Hills-Kimball, T. Cai, P. Wang, A. Tang and O. Chen, *Nano Lett.*, 2021, **21**, 1620–1627.
16 X. Zhu, Y. Lin, Y. Sun, M. C. Beard and Y. Yan, *J. Am. Chem. Soc.*, 2019, **141**, 733–738.
17 X. Zhu, Y. Lin, J. San Martin, Y. Sun, D. Zhu and Y. Yan, *Nat. Commun.*, 2019, **10**, 2843.
18 Z. Zhang, Y. Yang, Y. Wang, L. Yang, Q. Li, L. Chen and D. Xu, *Angew. Chem., Int. Ed.*, 2020, **59**, 18136–18139.
19 S. Park, W. J. Chang, C. W. Lee, S. Park, H.-Y. Ahn and K. T. Nam, *Nat. Energy*, 2016, **2**, 16185.
20 L. Ye, X. Jin, X. Ji, C. Liu, Y. Su, H. Xie and C. Liu, *Chem. Eng. J.*, 2016, **291**, 39–46.
21 S. Ma, W. Song, B. Liu, W. Zhong, J. Deng, H. Zheng, J. Liu, X.-Q. Gong and Z. Zhao, *Appl. Catal., B*, 2016, **198**, 1–8.
22 S. Sun, P. Gao, Y. Yang, P. Yang, Y. Chen and Y. Wang, *ACS Appl. Mater. Interfaces*, 2016, **8**, 18126–18131.
23 X. Y. Zhang, P. Wang, Y. Zhang, X. M. Cheng and W. Y. Sun, *ACS Appl. Mater. Interfaces*, 2023, **15**, 3348–3356.
24 Y. A. Wu, I. McNulty, C. Liu, K. C. Lau, Q. Liu, A. P. Paulikas, C.-J. Sun, Z. Cai, J. R. Guest, Y. Ren, V. Stamenkovic, L. A. Curtiss, Y. Liu and T. Rajh, *Nat. Energy*, 2019, **4**, 957–968.
25 H. Zhou, M. Wang, F. Kong, Z. Chen, Z. Dou and F. Wang, *J. Am. Chem. Soc.*, 2022, **144**, 21224–21231.
26 J. G. Yu, J. X. Low, W. Xiao, P. Zhou and M. Jaroniec, *J. Am. Chem. Soc.*, 2014, **136**, 8839–8842.
27 Y. Xu, A. Yan, X. Zhang, F. Huang, D. Li, X. Zhao, H. Weng and Z. Zhang, *Chem. Commun.*, 2021, **57**, 5774–5777.
28 Y. F. Si, K. Sun, X. L. Chen, X. Y. Fu, Y. Liu, F. L. Zeng, T. Shi, L. B. Qu and B. Yu, *Org. Lett.*, 2020, **22**, 6960–6965.
29 E. Vitaku, D. T. Smith and J. T. Njardarson, *J. Med. Chem.*, 2014, **57**, 10257–10274.
30 H.-M. Huang, M. H. Garduño-Castro, C. Morrill and D. J. Procter, *Chem. Soc. Rev.*, 2019, **48**, 4626–4638.
31 S. Y. Cheng, J. B. Liao, Y. M. Lin and L. Gong, *Org. Lett.*, 2023, **25**, 6566–6570.
32 S. Shyamal, S. K. Dutta, T. Das, S. Sen, S. Chakraborty and N. Pradhan, *J. Phys. Chem. Lett.*, 2020, **11**, 3608–3614.
33 L. Peng, S. K. Dutta, D. Mondal, B. Hudait, S. Shyamal, R. Xie, P. Mahadevan and N. Pradhan, *J. Am. Chem. Soc.*, 2019, **141**, 16160–16168.
34 J.-C. Wang, N. Li, A. M. Idris, J. Wang, X. Du, Z. Pan and Z. Li, *Sol. RRL*, 2021, **5**, 2100154.
35 Q. Guo, J. D. Zhang, Y. J. Chen, K. Y. Zhang, L. N. Guo, Q. C. Shan, J. L. Lu, X. H. Duan and L. Z. Wu, *Chem. Commun.*, 2023, **59**, 4189–4192.
36 H. Huang, H. Yuan, J. Zhao, G. Solís-Fernández, C. Zhou, J. W. Seo, J. Hendrix, E. Debroye, J. A. Steele, J. Hofkens, J. Long and M. B. J. Roeffaers, *ACS Energy Lett.*, 2018, **4**, 203–208.

